Measurement 186 (2021) 110153

Contents lists available at ScienceDirect

Measurement

journal homepage: www.elsevier.com/locate/measurement

An upgraded lab-based method to determine natural γ-ray emitters in NORM samples by using Ge detectors

A. Barba-Lobo *, F. Mosqueda, J.P. Bolívar

Radiation Physics and Environment Group (FRYMA), Department of Integrated Sciences, Center for Natural Resources, Health and Environment (RENSMA), University of Huelva, 21071 Huelva, Spain

ARTICLE INFO

Keywords:
Gamma spectrometry
Ge detectors
Efficiency calibration
NORM
Self-attenuation
^{222}Rn losses

ABSTRACT

The regulation existing on NORM activities requires the accurate and quick measurement of natural radionuclides in a wide range of matrices by gamma spectrometry. The aim of this work has been to develop a comprehensive and accurate methodology to determine natural long-lived radionuclides (^{210}Pb, ^{228,226}Ra, ^{234,228}Th and ^{40}K) by gamma spectrometry with Ge detectors in NORM samples. An exhaustive calibration method to obtain the full-energy peak efficiency (*FEPE*), for each gamma emission energy, as a function of the thickness, apparent density and matrix composition of the cylindrical sample, has been developed. The selected certified calibration standards contain only natural radionuclides belonging to the ^{238}U- and ^{232}Th-series as well as ^{40}K (codes RGU-1, RGTh-1 and RGK-1 from IAEA). Then, the obtained *FEPE* curves were validated using Genie 2000 simulations and Certified Reference Materials, for which the self-attenuation corrections were considered. Finally, a study on ^{222}Rn losses was done for several samples.

1. Introduction

In many problems related to the field of environmental radioactivity, the determination of long-lived gamma-ray emitting radionuclides such as $^{234,\ 228}$Th, $^{228,\ 226}$Ra, ^{210}Pb and ^{40}K is needed, in a wide variety of samples with different compositions and densities, as well as their geometry due to the available amount of sample is variable.

There are many industries (e.g., fertilizers, TiO_2 pigments, oil extraction, production of metals, mining) that generate intermediate materials, final products and wastes containing natural radionuclides at significant concentrations, and therefore they have to be considered as NORM (Naturally Occurring Radioactive Material) or TENORM (Technologically Enhanced NORM). The control of their potential radiological impact requires accurate methods for the measurement of natural radionuclides in industrial and environmental samples in a wide range of matrices with very different apparent densities, compositions and amount of sample, which requires different measuring geometries (thickness of sample) [1–3].

The Radiation Physics and Environment Group of the University of Huelva (Spain) has led many studies on radiological assessments of chemical NORM industries where a wide range of gamma-ray spectrometry measurements of TENORM samples is needed. TENORM samples contain ^{238}U- and ^{232}Th-series radionuclides, which are not in secular equilibrium, and therefore the separate measurement of ^{238}U (via ^{234}Th), $^{230,\ 228}$Th, $^{228,\ 226}$Ra, ^{210}Pb and ^{40}K radionuclides is essential. The issue related to the secular disequilibrium is very important to be analyzed since there are many types of samples such as phosphogypsum materials, industrial wastes (like scales) and waters that present a clear disequilibrium between the radionuclides belonging to the ^{238}U- and ^{232}Th-series. The most common disequilibrium cases usually occur between ^{238}U and ^{226}Ra as well as between ^{226}Ra and ^{222}Rn. (See [4–6] for further information about studies on secular disequilibrium).

Nowadays, NORM samples are being very important because society is more committed to environmental sustainability. Among the samples of interest are industrial wastes, which are studied to evaluate their radiotoxicity levels, ensuring that they are within the limits allowed to guarantee the safety of the workers who are exposed to the radiation from these wastes. Besides that, other samples such as waters, which are used to irrigate farm products, are analyzed to assure that they are suitable for consumption (further information about NORM samples can be found in [7,8]).

On the other hand, exposure to NORM samples can lead to health problems when they have high levels of radioactivity. For this, lately radiological regulations for construction require the measurement of

* Corresponding author.
E-mail address: alejandro.barba@dci.uhu.es (A. Barba-Lobo).

https://doi.org/10.1016/j.measurement.2021.110153
Received 14 August 2020; Received in revised form 11 August 2021; Accepted 7 September 2021
Available online 11 September 2021

radioactive NORM building materials to calculate parameters, such as the activity concentration index [9], radium-equivalent activity [10], or the external radiation hazard [11]. These radiological parameters require the measurement of ^{226}Ra, ^{232}Th and ^{40}K, where ^{226}Ra and ^{232}Th are easier to be determined if they are in secular equilibrium with ^{214}Pb (or ^{214}Bi) and ^{228}Ac, respectively. (See [12] for further information on contamination caused by NORM samples).

Regarding the ^{226}Ra, ^{232}Th and ^{40}K determinations, gamma spectrometry with high purity germanium (HPGe) detectors is the most useful radiometric technique. This kind of detectors must be calibrated with a reference sample that has the same geometry than the one used for the real samples. For that, this study is focused on finding, for every gamma emission of interest, a general efficiency function obtained for the calibration matrix and depending on the sample thickness for a cylindrical geometry. Regarding the specific ranges, it is necessary that the radius of that geometry is smaller than the one of the detectors. On the other hand, those radionuclides previously mentioned can be determined by medium resolution detectors, for example, $CeBr_3$ detectors. However, in contrast to the HPGe detectors, the activity concentration calculations carried out using medium resolution detectors have very high uncertainties due to their lower resolution [13–16]. Consequently, the radionuclide determinations can be accomplished in a more accurate way using HPGe detectors.

On the other hand, nowadays the calibration of detectors by using MCNP, GEANT4, PENELOPE or FLUKA simulation codes has become generalized [17–21]. However, for this, it is necessary to carry out the "characterization" of the detector parameters, which implies a very expensive process developed by the manufacturer, being the detector inoperative and out of the laboratory during several months. Considering this problem as well as all the previous ones, this work is focused on obtaining the full-energy peak efficiency (*FEPE*) for a detection system with a HPGe detector for the certified calibration matrix (ε_c), which depends on the peak energy of interest, and the sample thickness in cylindrical geometry (h), covering the range of energies for natural radionuclides (from 46.5 keV to 1764.5 keV). The efficiency curve found for the calibration sample (ε_c), must be corrected due to the different gamma self-attenuation between the calibration and problem samples. Besides, a study on the "sensitivity" of the method has also been carried out as a function of the parameters for which the measurement is accomplished.

2. Materials and methods

In order to carry out this study, an extended range high purity germanium detector (XtRa) was employed. This spectrometric system also incorporates a device that introduces evaporated nitrogen from the Dewar into the shield, displacing the air initially contained and, consequently, the radon present in it. The XtRa detector has a relative efficiency of 38.4 % in relation to a 3″ × 3″ NaI (Tl) detector, a full width at half maximum (FWHM) of 1.74 keV and 0.88 keV at 1332 keV and 122 keV, respectively, and a peak-to-Compton ratio of 67.5:1. Then, regarding the necessary environment conditions in the laboratory in order to carry out the methodology proposed in this study, they are the following: 1. The detectors and shielding should contain the minimum concentrations of radioactive impurities; 2. The temperature inside the laboratory need to be approximately 20 °C; and 3. The ^{222}Rn concentrations need to be as low as possible in indoor air, being the daily average concentration about 10 Bq m^{-3}.

On the other hand, a conventional electronic chain is connected to the HPGe detector to obtain the gamma spectra by the Genie 2000 software. This software belongs to Canberra Industries and it is one of the packages most used for the analysis as well as for the data acquisition in gamma spectrometry, demonstrating the reliability of this software [22,23]. In order to analyze the gamma spectra, this software employs algorithms which can be consulted in [24].

To determine the experimental efficiencies, standards provided by the IAEA (RGU-1, RGTh-1 and RGK-1) have been used, which are Certified Reference Materials (CRM) and contain natural radionuclides from ^{238}U-series, ^{232}Th-series, and ^{40}K, whose certified activity concentrations were 4940 ± 15 Bq kg^{-1}, 3250 ± 45 Bq kg^{-1}, and 14000 ± 200 Bq kg^{-1}, respectively, being the uncertainties given at one sigma level. The RGU-1 and RGTh-1 standards were prepared by the Canada Centre for Mineral and Energy Technology by dilution of a uranium ore BL-5 (7.09 % U) and a thorium ore OKA-2 (2.89 % Th, 219 μg U g^{-1}) with floated silica powder of similar grain size distribution, respectively, and no evidence of inhomogeneity was detected after mixing and bottling. Therefore, for both standards there is no disequilibrium problem, confirming that all the radionuclides contained in them are in radioactive equilibrium [25,26]. Regarding the RGK-1, it was produced from high purity (99.8 %) potassium sulphate provided by the Merck Company. The ^{40}K concentration and its uncertainty were obtained from repeated measurements performed at the IAEA Laboratories in Seibersdorf and the results confirmed the value certified by Merck [26].

Once the most intense gamma emissions of these standards were selected, an apparent density of 1.63 ± 0.02 g cm^{-3} was obtained after compacting them until reaching the chosen thickness values (from 5 to 50 mm and from 5 to 45 mm with intervals of 5 mm in the cases of RGTh-1 and RGK-1, and RGU-1 standards, respectively). Then, the experimental *FEPE* values at the different selected gamma energies and thicknesses were calculated. The experimental *FEPE* values calculated in the calibration standard matrices as well as the gamma emission probabilities related to the selected energies were shown in Tables A.1 and A.2 (both in Supplementary Information). After the experimental *FEPE* calculations, the simplest empirical *FEPE* function depending on the thickness was obtained for each selected energy. Finally, the efficiency calculated in the standard matrices (ε_c) must be determined in the problem sample (also called as real sample) matrices. For this, the so-called self-attenuation factor (f) needs to be employed, which depends on the chemical compositions, thickness of the real sample (h, which is also called as the sample hight) and apparent densities of both the standard and the real sample, obtaining the efficiency in the real sample matrix (ε).

The validation of the efficiency curves was done by means of samples whose concentrations of natural radionuclides were known. Furthermore, the methodology proposed in this study has been validated using CRMs which were employed in Inter-Comparison exercises. In this kind of exercise, it is necessary to follow a protocol in order to prepare the samples before measuring them. Regarding the reference values resulted from the Inter-Comparison exercises, they are obtained considering all the calculations provided by each laboratory and taking a mean value of them (see [27] for further information on Inter-Comparison exercises). On the other hand, a study on ^{222}Rn losses in certified materials, such as phosphogypsum materials and dissolved RGU-1 standard, was carried out calculating the ^{226}Ra activity concentration by using either the gamma emissions of the ^{222}Rn daughters, that is, ^{214}Pb and ^{214}Bi, or its gamma emission of 186 keV, subtracting the interference from ^{235}U.

3. Results and discussion

3.1. Full-energy peak efficiency (FEPE) curves for the calibration matrix

The experimental *FEPEs* obtained in the calibration sample matrices (ε_c^{exp}) have been calculated by the following equation:

$$\varepsilon_c^{exp}(E_\gamma, h) = \varepsilon_c^{exp}(E_\gamma, m_c) = \frac{G - B - F - I}{P_\gamma \; a \; m_c \; t} \quad (1)$$

where G, B, F, and I are the total number (gross) of counts for the full-energy peak of interest, the Compton continuum, the background due to environmental conditions in the laboratory and the interference term, respectively. Then, P_γ is the probability of gamma emission (taken from [28]), a, m_c and h are the activity concentration, mass and height of the

standard, respectively, used in the calibration procedure, E_γ is the gamma emission and t is the measurement time. It has been considered that $I \sim 0$, this being one of the requirements in the gamma emission selection. Besides, it is necessary to clarify that the *FEPE* given by Eq. (1) is an apparent full-energy peak efficiency since the true coincidence-summing corrections have not been included. Thus, from now on, let us call the apparent *FEPE* as *FEPE* in order to abbreviate the name of this type of efficiency.

Firstly, the *FEPE* function depending on the height for each gamma emission was obtained. The mass/ height ratio in the preparation of the standards was constant (about 7.5/5.0 = 1.50 g mm^{-1}), obtaining a constant apparent density, ρ_c, of about 1.63 g cm^{-3} ($\rho_c = m_c/\pi r^2 h$), being r the radius of cylindrical geometry of the standards.

In Tables A.1 and A.2, it is possible to see that the uncertainties given at 1 sigma level for the experimental efficiencies ranged from 1 % to 3 %, where the uncertainty related to the counting rate was the greatest contribution to the efficiency uncertainties. Besides, the uncertainty associated to the sample height, $\sigma(h)$, was also taken. However, considering $\sigma(h) = 0.2$ mm (heights measured using a high precision caliper), $\sigma(h)$ can be completely neglected compared with the one related to the counting rate.

On the other hand, in the case of the RGU-1 standard, it is known that the activity ratio $^{235}U/^{238}U = 0.046$, $P_\gamma(^{226}Ra) = 0.0351(6)$ and $P_\gamma(^{235}U) = 0.572(5)$ at 186 keV. Therefore, when the secular equilibrium between ^{238}U and ^{226}Ra is considered, an equivalent probability at this energy of $P_\gamma(^{226}Ra + {}^{235}U) = 0.0614(6)$ can be taken.

In Figs. 1 and 2, the experimental *FEPEs* versus h values in logarithmic scale were shown, observing that the majority of the curves are parallels, except for low energy emissions such as 46 keV and 63 keV, increasing the deviation as the energy decreases and finding the maximum deviation for 46 keV (^{210}Pb). This occurs because of the significant differences between self-attenuation corrections provided at low and high energies (>150 keV), since within the high energy zone the self-attenuation effects are less relevant than the ones corresponding to the low energy zone. The corrections due to the different self-attenuation effects in the case of the calibration standards compared with the one related to the real samples will be studied in Section 3.2.

There are some singular cases at 129 keV, 583 keV, 609 keV, 768 keV, 934 keV, 1120 keV and 1238 keV since the *FEPE* values for these energies are lower than the expected ones, being 583 keV, 609 keV and 1120 keV one of the most employed energies in order to determine ^{226}Ra (609 keV and 1120 keV) and ^{228}Th (583 keV). This fact can be explained due to the significant true coincidence summing effects (TCS) existing for those three gamma emissions (see [29–31]), and this corroborates that for natural radionuclides is better to calibrate fixing the energy. As it is well known, the TCS effects decrease as the sample height increases (distance detector-sample), which are observed in Figs. 1 and 2, where it is possible to realize that the efficiency values for 583 keV, 609 keV and 1120 keV are closer than the expected ones as the sample height increases. This occurs in this way because as the sample height increases, the absolute efficiency (ε_{ab}) decreases occasioning a diminution of the TCS effects, since ε_{ab} and the TCS effects are related to each other (see [32] for further information about the relationship between ε_{ab} and TCS effects). However, the TCS effects are not a problem in our calibration procedure, since it has been carried out varying the height and fixing the energy. Consequently, the fact that the 583 keV, 609 keV and 1120 keV and all the other energies mentioned in this paragraph present TCS effects does not affect the quality of our activity concentration calculations.

The best fitting for ε_c will be an asymptotic exponential function as follows:

$$\varepsilon_c(E_\gamma, h) = ar_1 exp(ar_2 h) + ar_3 \quad (2)$$

where ar_1, ar_2 and ar_3 are parameters obtained after fitting the experimental *FEPEs* versus h, being h the sample height. The fittings given by Eq. (2) were compared statistically by finding their confidence intervals with the method described in [33]. Besides, note that in Eq. (2) the efficiency value is $ar_1 + ar_3$ or ar_3 when h is relatively small or large, respectively, as it is expected from the *FEPE* behavior for the particular range of h (from 0.5 to 5 cm). The ar_2 parameter must be negative since

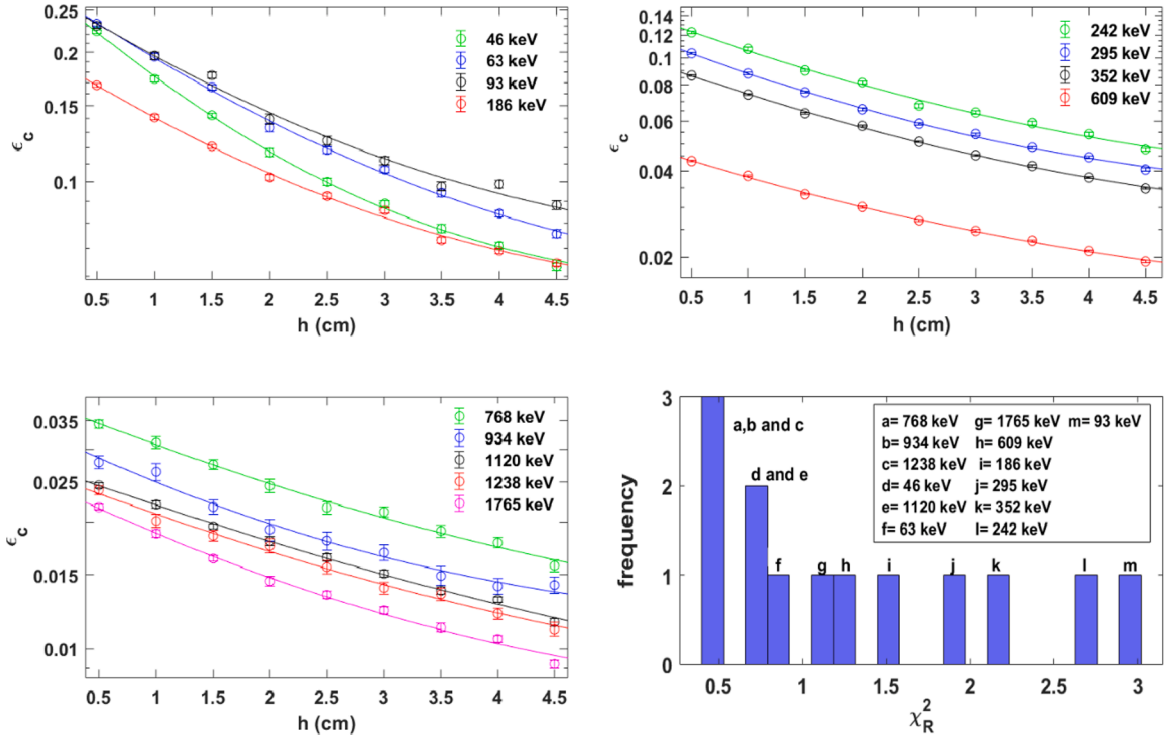

Fig. 1. Experimental ε_c values versus height for RGU-1 standard fixing E_γ and histogram of reduced chi-square values (critical χ^2_R is 2.1 at 0.05 of significance level (α) and 6 degrees of freedom (ν)) obtained after fittings.

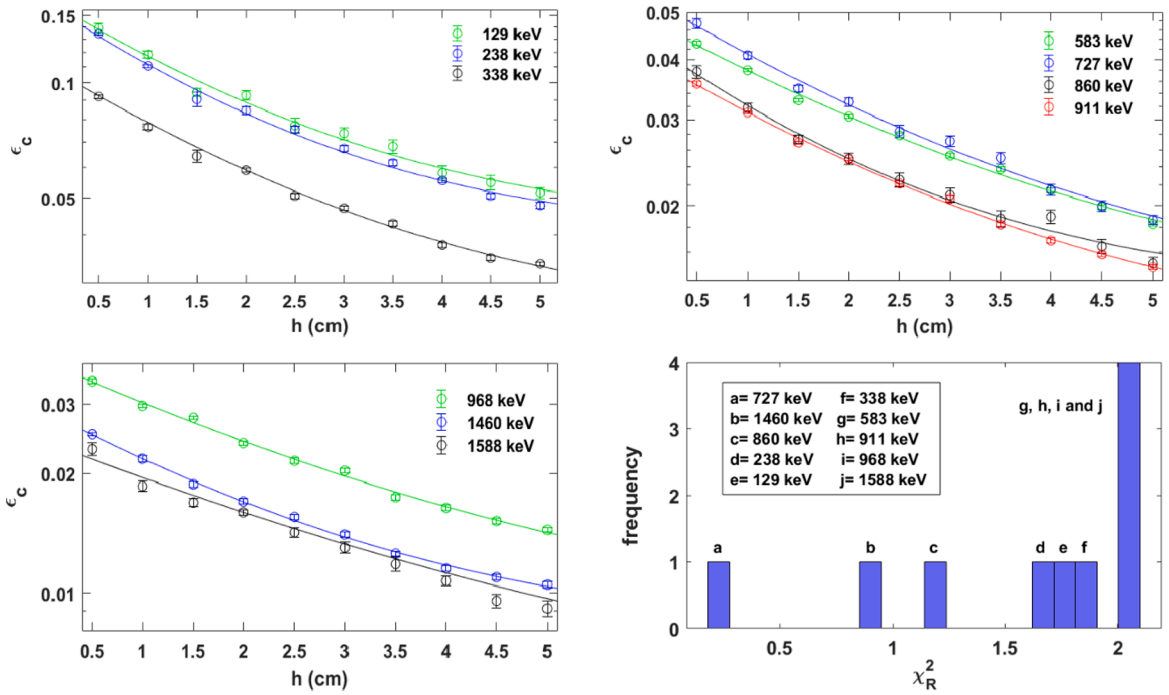

Fig. 2. Experimental ε_c values against height for RGTh-1 and RGK-1 standards fixing E_γ and histogram of reduced chi-square values (critical χ^2_R is 2.01 at 0.05 of significance level (α) and 7 degrees of freedom (ν)) obtained after fittings.

the efficiency decreases as h increases.

The fittings provided by Eq. (2) (continuous lines in Figs. 1 and 2) are in very good agreement with the experimental data, obtaining values for the reduced chi-square (χ^2_R) which are lower than the critical value (2.1 or 2.01 in the cases of Figs. 1 and 2, respectively) at 0.05 of significance level for the majority of the cases (see histograms in Figs. 1 and 2) [34].

Tables A.3 and A.4 (both in Supplementary Information) show the values of the ar_1, ar_2 and ar_3 parameters obtained after fitting experimental efficiencies which have been calculated in the calibration matrix of RGU-1 and RGTh-1 and RGK-1, respectively. The uncertainties of these parameters (calculated at one sigma level) were ranged from 1 to 3 %, 5–7 % and 4–6 % for ar_1, ar_2 and ar_3, respectively, in the case of RGU-1 standard while these values were ranged from 1 to 4 %, 4–7 % and 4–6 % for ar_1, ar_2 and ar_3, respectively, in the cases of RGTh-1 and RGK-1 standards. Regarding these uncertainties, it is interesting to realize that the relative uncertainty associated with ar_2 is usually higher than the ones related to the other parameters. On the other hand, regarding the relative average residues, $<Res>$, obtained at each energy (Tables A.3 and A.4) are very useful to evaluate the *FEPE* relative uncertainty obtained from the fitting functions. These $<Res>$ values ranged from 0.8 % (352 keV) to 3.9 % (129 keV), confirming the very good fittings obtained for *FEPE*.

Regarding the calculation of experimental efficiency values in the calibration matrices, we have considered that it would be appropriate to compare these values with the ones calculated by Genie 2000 simulations. This comparison was made to check the validity of the algorithm used by this software, being possible at the same time to verify that the calculations of these experimental efficiencies were carried out correctly. Thus, some energies have been selected in order to make this comparison (63 keV, 352 keV, 609 keV and 1120 keV in the case of the RGU-1 standard and 238 keV, 583 keV, 911 keV and 1460 keV in the cases of RGTh-1 and RGK-1 standards). Then, the z_{score} values were calculated for each height and finally it has been averaged over all these values, obtaining an average z_{score} value ($<z_{score}>$) for each energy, where the expression used to calculate each z_{score} value has been as follows:

$$z_{score} = \frac{|a_1 - a_2|}{\sqrt{\sigma(a_1)^2 + \sigma(a_2)^2}} \quad (3)$$

where a_1 and a_2 are the two compared values and $\sigma(a_1)$ and $\sigma(a_2)$ their respective uncertainties calculated at one sigma level.

As can be seen in Tables A.5 and A.6 (both in Supplementary Information), the large majority of the z_{score} values obtained for each height were below 1 for the calculations carried out in the RGU-1, RGTh-1 and RGK-1 calibration matrices. In addition, all the $<z_{score}>$ values were below 0.5 for the three calibration matrices, so the algorithm used by Genie 2000 to calculate the efficiency values works correctly and it has also been verified that the calculations of the experimental efficiencies have been carried out correctly.

3.1.1. *FEPE fittings versus height (E_γ = constant); comparison with other studies*

In this Section, the reasons for the selection of the fitting function given by Eq. (2) have been analyzed. Previous works [35–38] were carried out to assess the *FEPE* varying h and fixing E_γ but using a pure exponential function as:

$$\varepsilon_c(E_\gamma, h) = br_1 exp(br_2 h) \quad (4)$$

where br_1 and br_2 are the parameters used to fit the experimental efficiencies.

Some of the most intense gamma energies covering the full energy range were selected, these being 63 keV, 352 keV, 911 keV and 1460 keV (belonging to ^{234}Th, ^{214}Pb, ^{228}Ac and ^{40}K, respectively). The fittings obtained by Eqs. (2) and (4) were shown in Fig. 3.

It is easy to realize that the pure exponential function (function B in Fig. 3) does not fit properly to the experimental data, especially for the extreme heights, that is, at 5 mm and at 45 or 50 mm. However, our function (A in Fig. 3) agrees very well with the experimental efficiencies since they continue behaving as an asymptotic function even though the efficiency has been represented using logarithmic scale.

Table A.7 (in Supplementary Information) shows the parameters resulted from the fittings carried out by function B as well as the $<Res>$

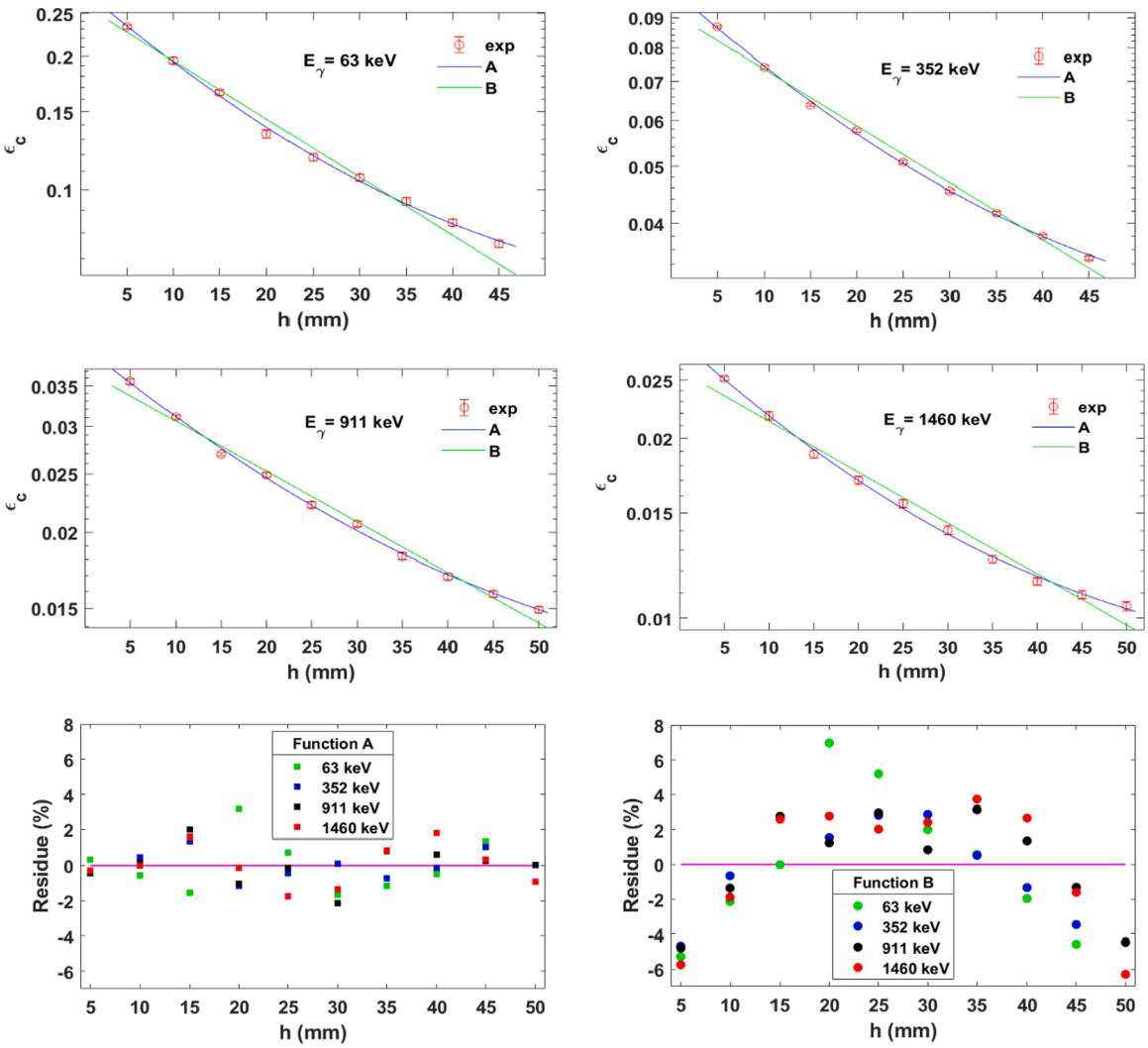

Fig. 3. Comparison between fittings of the experimental efficiencies versus height, where fittings carried out by two function types and their respective relative residues have been shown: A (used in this work) and B (used in previous works).

and χ^2_R values obtained after fitting by both functions. The total relative average residue, $< Res >_T$, for the fittings done by function B was 3.4 %, while the one obtained by function A was 1.2 %. Furthermore, the χ^2_R values obtained for function B were very much higher than the critical tabulated one (χ^2_R is 1.94 at 0.05 of confidence level (α) and 8 degrees of freedom (ν)), while the χ^2_R values obtained for function A were close or smaller than the tabulated ones (see Table A.7). Therefore, it has been proven that function A (used in this study) works much better than function B (used in previous works) and, consequently, for this reason, function A was chosen.

3.1.2. FEPE versus energy (h = constant) compared to FEPE versus height (E_γ = constant)

In this Section, we justify the reasons why an efficiency calibration method in which the height is varied and the energy is fixed for the different natural radionuclides has been selected. For this, the *FEPEs* obtained by our function (*FEPE* vs height) have been compared with the ones obtained using the most common fitting functions resulted from the *FEPE* versus energy. Thus, the function selected was [29,39–42]:

$$\varepsilon_c(E_\gamma, h) = \exp\left(\sum_{i=1}^{4} cr_i \ln(E_\gamma/E_0)^{i-1}\right) \quad (5)$$

where cr_i are the parameters resulted from the fittings by the cubic polynomial function, whose values are shown in Table A.8 (in Supplementary Information) and E_0 = 1 keV. Thus, Eq. (4) will be called "function C".

The gamma emissions corresponding to the radionuclides that belong to ^{238}U-series (radionuclides contained in RGU-1) were selected for this comparison, since these energies are uniformly distributed throughout the range of low and high energies. In Fig. 4 it is possible to see the graphics of the experimental efficiency fittings done by the logarithm of function C for an energy range that goes from 46.5 keV to 1764.5 keV and for heights ranged from 5 mm to 45 mm. In these graphics, the experimental efficiency values tend to deviate somewhat from the expected values. This occurs because when calibration in efficiency is carried out varying the energy, the TCS effects are more relevant, so the efficiency values usually deviate from the ones given by the fitting function in this type of calibration. This requires corrections due to the TCS effects. However, doing the calibration in efficiency varying the height and fixing the energy, it is not necessary to take this type of problem into account.

On the other hand, it is interesting to note that when a calibration in efficiency varying E_γ is done, the uncertainties related to the emission probability, $\sigma(P_\gamma)$, must be considered. This occurs in this way because applying this calibration method, E_γ is varied and, consequently, $\sigma(P_\gamma)$ is not possible to be considered as a systematic uncertainty. This implies that for this calibration method, the uncertainties of the experimental

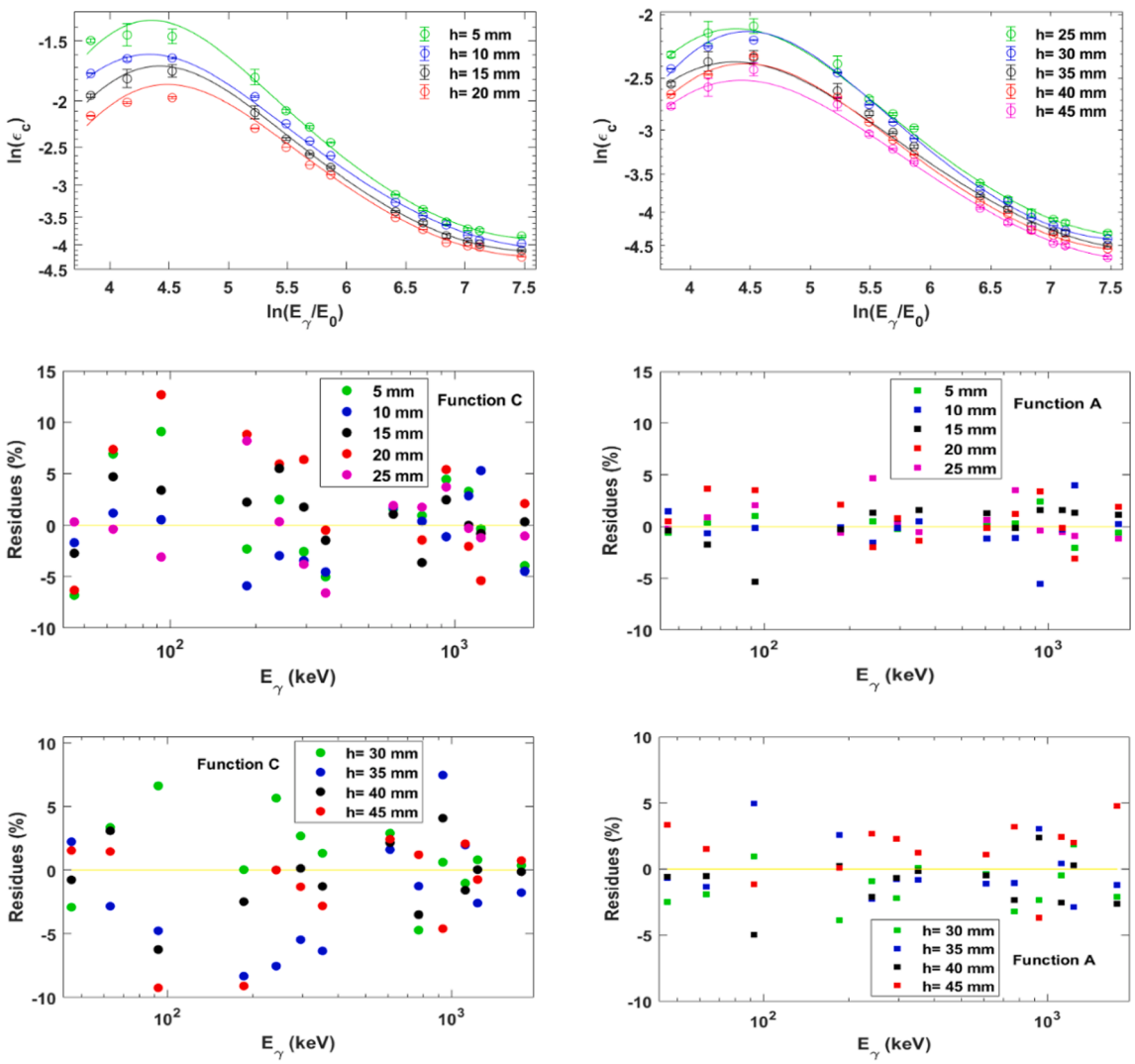

Fig. 4. Fittings of *FEPE* versus energy carried out by function C. Besides, the residues resulted from the fittings done using function C (left column) were compared with the ones obtained by using function A (right column).

efficiencies are much higher than the ones obtained when a calibration varying h is carried out. Thus, the relative values of $\sigma(P_\gamma)$ ranged from 0.2 % (for 352 keV (^{214}Pb)) up to 9 % (for 93 keV (^{234}Th)).

The relative residues are very useful to assess the goodness of the fitting functions. Thus, as can be seen in Fig. 4, after fitting by function C, the obtained residues were much higher than the ones obtained by function A for all the chosen E_γ and h values (1–6 % and 0–3 %, respectively). Table A.8 shows the $<Res>$ values at each h value for both functions A and C. Note that for all the h values, $<Res>$ values were about double in the case of the function C in comparison with the ones obtained by function A, getting a $< Res >_T$ value of 4.5 % and 2.2 %, respectively. Therefore, it is possible to conclude that the function proposed in this work (function A) provided much better results of the *FEPE* fittings in comparison with the ones provided by the traditional function used in the majority of studies (function C). It is necessary to emphasize that this is possible in the case of NORM samples because the assessment of the activity of each radionuclide in the sample is done with reference to the activity of the same radionuclide in the calibration source. When this type of relative measurement is not possible, the efficiencies corrected due to TCS effects, which depend smoothly on energy, should be fitted as a function of energy for the calculation of the *FEPE* for the energies of interest.

3.2. *FEPE curves for real samples; corrections due to self-attenuation effects*

The measurement of real samples requires to include corrections because the self-attenuation of the gamma radiation in the real sample matrix is different from the one corresponding to calibration samples. In order to carry out this correction, it is necessary to introduce the so-called self-attenuation correction factor (f), which is defined as the ratio of the number of photons coming out from the real sample and the number of photons coming out from the standard that are recorded in the full-energy peak [43–47]. Thus, the self-attenuation factor would be expressed mathematically like this:

$$f = N/N_c = \varepsilon/\varepsilon_c \tag{6}$$

where N_c and N are the number of photons detected in the peak from the calibration and real samples (both with the same activity), respectively, and ε_c and ε are the efficiencies calculated in the calibration and real matrices, respectively.

According to [32,48], assuming cylindrical geometry, only the photons parallel to the symmetry axis are detected, and the activity is homogenously distributed in the sample, the number of detected photons (N) can be calculated as:

$$N = N_0 \frac{1 - exp(-\eta\rho h)}{\eta\rho h} \tag{7}$$

where N_0 is the number of photons detected from the sample without attenuation, and ρ, η, h are the density, the mass attenuation coefficient and the sample height for the measuring geometry, respectively. It is necessary to clarify that in Eq. (7) the non-coaxial photons are also considered, being the only approach that the real distance travelled by the detected oblique photons is replaced by the parallel one. Due to the angle between the photon trajectory and the coaxial axis of the detector is very small, the difference between both the real and coaxial distances will be negligible.

If we consider the same measuring geometry for both calibration and problem samples, the self-attenuation factor (Eq. (6)) can be written by:

$$f = N/N_c = \frac{\eta_c\rho_c(1 - exp(-\eta\rho h))}{\eta\rho(1 - exp(-\eta_c\rho_c h))} = f(E_\gamma, h, x_i) \tag{8}$$

where h and E_γ are the real sample height and the energy for which the self-attenuation correction factor is calculated, and x_i is the proportion of each chemical element (i) in both the real and calibration samples, since their mass attenuation coefficients depend on their chemical compositions. It is necessary to clarify that in Eq. (8), the heights of the calibration and real samples are considered the same, that is, h.

Therefore, the efficiency calculated for the real sample (ε) will be given by:

$$\varepsilon = f(E_\gamma, h, x_i)\varepsilon_c(E_\gamma, h) \tag{9}$$

where $\varepsilon_c(E_\gamma, h)$ and $f(E_\gamma, h, x_i)$ are the efficiency in the calibration matrix and the self-attenuation correction factor, respectively.

The average mass attenuation coefficient for each energy and composition can be calculated by using the so-called Bragg's law as follows:

$$\langle\eta\rangle = \sum_i x_i\,\eta_i \tag{10}$$

where x_i and η_i are the proportion and the mass attenuation coefficient of each chemical element at a specific energy, respectively (η_i values taken from [49]). Alternatively, the mass or the linear attenuation coefficients for any element, compound or mixture can be directly evaluated using [43,50].

3.3. Calculations of the minimum detectable activity concentrations for NORM samples

In this Section, it has been carried out a study on the dependence of the minimum detectable activity concentration (*mda*) on the type of sample, height sample and energy. The *mda* is defined as the minimum concentration that a sample needs to have in order to be detected over a background with a significance level (α, this being equal to 0.05 in our case). The *mda* can be calculated by the following equation:

$$mda = \frac{LLD}{\varepsilon\ m\ P_\gamma\ t} \tag{11}$$

where *LLD*, ε, m and P_γ are the lower limit of detection, the efficiency calculated in the real sample matrix, the real sample mass and the emission probability, respectively, referred to a specific energy and t is the counting time. The equation that defines *LLD* considers the existence or absence of interferences in gamma emissions (equations taken from [51,52]).

The interference term (I) is often neglected for most chosen gamma emissions. However, in this Section the gamma emission of 186 keV has been analyzed, which belongs to ^{226}Ra, in the cases where ^{226}Ra and ^{238}U are and are not in secular equilibrium. In the latter case, the interference between ^{226}Ra and ^{235}U (I_{235U}) must be considered, and it is given by the following equation:

$$\begin{aligned} I_{235U} &= A_{235U}\ P_\gamma(235U)\ \varepsilon_{186keV}\ t \\ &= 0.0263\ A_{238U}\ \varepsilon_{186keV}\ t \end{aligned} \tag{12}$$

where A_{235U}, A_{238U} are ^{235}U and ^{238}U activities, respectively, $P_\gamma(^{235}U)$ is the emission probability of ^{235}U at 186 keV, ε_{186keV} the efficiency calculated in the real sample matrix at 186 keV and t is the counting time.

In Eq. (12), $A_{235U} = 0.046A_{238U}$ has been considered [53]. Besides that, if secular equilibrium between ^{234}Th and ^{238}U is also considered, it would be possible to write $A_{238U} = A_{234Th}$, and since A_{234Th} can be calculated using ^{234}Th (63 keV), the interference I_{235U} can be determined.

Thus, the *mda* behavior was analyzed for different selected NORM samples: RGU-1, RGTh-1 and RGK-1 standards, phosphogypsum samples provided by IAEA (IAEA-434) and used in the CSN/CIEMAT Intercomparison carried out in 2008 (CSN-PG), as well as two scales named Scale-1 and Scale-2. Regarding CSN and CIEMAT, they are the acronyms for the Spanish Nuclear Safety Council ("Consejo de Seguridad Nuclear") and the Centre for Energy, Environment and Technology Research ("Centro de Investigaciones Energéticas, Medioambientales y Tecnológicas"), respectively.

Firstly, it has been shown the comparison between the *mda* behavior fixing the sample and varying the sample height (h = 10, 25 and 45 mm), that is, an internal comparison. The samples chosen for this case were the three standards: RGU-1, RGTh-1 y RGK-1. Then, it has been made an external comparison between the *mda* values obtained considering different samples for the same height (h = 25 mm), which has been carried out for the three standards as well as the other samples mentioned above (phosphogypsum and scale samples). The energy emissions chosen to make both types of comparisons were: 46.54 keV, 63.29 keV, 185.96 keV, 295.22 keV, 351.93 keV, 609.31 keV, 1120.29 keV (RGU-1 case), 238.63 keV, 338.42 keV, 583.19 keV, 911.16 keV (RGTh-1 case) and 1460.83 keV (RGK-1 case).

In both comparison types, a common counting time of 172,800 s was established, that is, two days. Regarding the apparent densities of each real sample, they are as follows: 0.71 g cm^{-3} (IAEA-434), 1.27 g cm^{-3} (CSN-PG), 1.32 g cm^{-3} (Scale-1) and 1.00 g cm^{-3} (Scale-2).

In Fig. 5 (left side), the *mda* values clearly decrease as the standard height (mass) increases, which is consistent because *mda* is inversely proportional to the sample mass. This *mda* behavior was the same for the great majority of the radionuclides contained in each standard. On the other hand, regarding the two cases corresponding to ^{226}Ra (with and without secular equilibrium between ^{226}Ra and ^{238}U), *mda* values were higher in all cases when secular equilibrium was not considered. This is also consistent because in the case of not considering secular equilibrium, the interference term (Eq. (12)) must be taken into account and, consequently, *mda* value increases.

Then, in Fig. 5 (right side), it can be seen what happens when different sample types are analyzed for the same height. Thus, the *mda* has a clear dependence on the properties of the analyzed samples, where the activity and density are the two factors that mainly contribute to the *mda* value. Regarding the activity, the *mda* specifically depends on the activity of ^{226}Ra and ^{228}Th, since if the Compton continuum at energies belonging to their daughters (^{214}Bi (1765 keV) and ^{208}Tl (2615 keV), respectively) is relatively large, the Compton continuum and, consequently, the *mda* value will also be relatively large for all the other energies. In the cases of radionuclides belonging to the ^{238}U-series, the *mda* behavior was very similar for all these radionuclides, being in the majority of the cases the highest *mda* value corresponding to the Scale-1 sample and followed by RGU-1, Scale-2, PG-IAEA and PG-CSN. On the other hand, for the cases corresponding to the radionuclides belonging to the ^{232}Th-series, there is a clear distribution of the *mda* values for the energies of 238 keV and 338 keV, with the largest value being obtained for Scale-1 and followed by Scale-2, RGTh-1, PG-IAEA and PG-CSN.

Finally, regarding the values corresponding to the ^{40}K *mda*, the

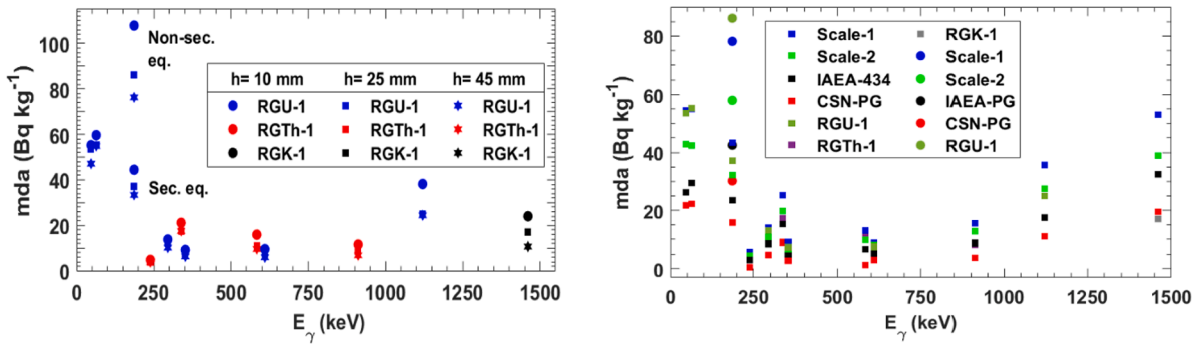

Fig. 5. (Left side) *mda* values obtained by fixing the sample type and varying the height (Non-sec. eq.: Non-secular equilibrium, Sec. eq.: Secular equilibrium at 186 keV); (Right side) *mda* values fixing the sample height (h = 25 mm) and varying the sample type (Non-sec. eq. (circles), Sec. eq. (squares)).

highest *mda* value is the one obtained for Scale-1 and followed by Scale-2, PG-IAEA, PG-CSN and RGK-1. In this case, it has been observed that the *mda* value of RGK-1 standard was the smallest. This is reasonable since the RGK-1 standard has a relatively small Compton continuum at 1460 keV and given that the *mda* is related to the Compton continuum counts, it is completely consistent that the *mda* value for this standard was less than the one obtained for the other samples. In the case of the RGK-1 standard, it has been verified that the number of counts belonging to the full-energy peak is 2 or 3 orders of magnitude higher than the one related to the Compton continuum.

3.4. Validations of the efficiency calibration methodology for NORM samples

Two kinds of validations have been considered: 1. External and 2. Internal (consistency test) validations. The first kind has been done using CRM samples, while the second one using uncertified samples, verifying that the activity concentration value of a specific radionuclide is very similar regardless of the E_γ and h values chosen to carry out its determination, that is, the second type of validation is a consistency test of the methodology proposed in this study.

In addition, note that the ^{226}Ra activity concentration ($a_{226\mathrm{Ra}}$) can be calculated considering non-secular equilibrium between ^{226}Ra and ^{238}U. At 186 keV (^{226}Ra + ^{235}U emissions), for NORM samples where ^{235}U/^{238}U activity ratio is 0.046, $a_{226\mathrm{Ra}}$ is given by the equation:

$$a_{226\mathrm{Ra}} = \frac{G - B - F - I_{235U}}{P_\gamma(226Ra)\ \varepsilon_{186keV}\ m\ t} = \frac{G - B - ft}{0.0351\ m\ \varepsilon_{186keV}\ t} - 0.75\ a_{234Th} \qquad (13)$$

where G and B are the gross and the Compton continuum of the 186 keV peak, respectively,I_{235U} is the interference term previously defined in Eq. (12) and P$_\gamma$(^{226}Ra) is the ^{226}Ra emission probability at 186 keV. Then, F and f are the environmental background expressed in counts and counts per second, respectively. On the other hand, ε_{186keV} is the efficiency calculated in the real sample matrix at 186 keV, t is the counting time, m is the sample mass and a_{234Th} is the activity concentration for ^{234}Th. In Eq. (13) it has been considered that ^{238}U and ^{234}Th are in secular equilibrium.

3.4.1. External validation

The following certified NORM samples: IAEA-326 (Soil), IAEA-434, CSN-PG and K_2CO_3, were selected because of their different apparent densities and chemical compositions, whose densities (heights) are as follows: 1.21 g cm^{-3} (25.1 mm), 0.70 g cm^{-3} (7.6 mm), 1.27 g cm^{-3} (15.4 mm) and 1.13 g cm^{-3} (9.1 mm), respectively.

In Table 1, the obtained $|z_{score}|$ values can be found, being below 2 in general, i.e., there was no significant differences between our measured and the reference values. In the case of the two phosphogypsum samples, the z_{score} values were very good for ^{234}Th and ^{210}Pb, while the z_{score} values for ^{226}Ra daughters were very bad in general. This happens because the phosphogypsum samples have a considerable percentage of ^{222}Rn losses from their grains, and they were measured immediately after their preparations, so ^{222}Rn was not in secular equilibrium with ^{226}Ra. However, if the ^{226}Ra activity concentration is determined by its gamma emission of 186 keV, a very good z_{score} value is obtained. Later, in Section 3.5, the analysis of the ^{222}Rn losses in phosphogypsum samples will be analyzed.

3.4.2. Internal validation

The following NORM samples were chosen, where the followed choice criteria were the same than the ones considered in the first validation type: Scale-1, Scale-2, Tionite and Ilmenite, whose densities (heights) are as follows: 1.32 g cm^{-3} (12.2 mm), 1.00 g cm^{-3} (13.9 mm),

Table 1
External validation for several NORM samples (IAEA-326, IAEA-434, CSN-PG and K_2CO_3, where in the case of K_2CO_3 sample, the calculated ^{40}K activity concentration has been 17462(478) Bq kg^{-1} and the reference value was 17800(255) Bq kg^{-1}, obtaining a z_{score} value of −0.6).

RN	E_γ(keV)	IAEA-326			IAEA-434			CSN-PG		
		a (Bq kg^{-1})	Reference(Bq kg^{-1})	z_{score}	a (Bq kg^{-1})	Reference (Bq kg^{-1})	z_{score}	a (Bq kg^{-1})	Reference (Bq kg^{-1})	z_{score}
^{234}Th	63.29	28(3)	29.4(1.7)	−1.4	156(38)	120(6)	0.9	38(14)	48.6(1.2)	−0.7
^{226}Ra	185.96 (Non-sec. eq.)	40(3)	33(3)	1.5	766(61)	780(31)	−0.2	614(37)	634(13)	−0.5
	185.96 (Sec. eq.)	34(3)		0.4	498(40)		−5.6	363(31)		−8.2
^{214}Pb	295.22	30.6(9)		−0.6	664(24)		−3.0	536(17)	580(13)	−2.1
	351.93	31.0(8)		−0.5	648(20)		−3.6	555(15)		−1.3
^{214}Bi	609.31	30.8(8)		−0.6	631(21)		−4.0	535(16)	533(13)	0.1
	1120.29	30.8(1.7)		−0.5	611(46)		−3.1	557(29)		0.7
^{210}Pb	46.54	38(2)	53(5)	−2.7	745(39)	680(29)	1.3	738(31)	781(15)	−1.4
^{228}Ac	338.42	42(7)	40(2)	0.2						
	911.16	40.3(1.3)		0.1						
^{212}Pb	238.63	37.8(9)	39.1(1.7)	−0.7						
^{208}Tl	583.19	37.4(1.1)		−0.9						
^{40}K	1460.83	592(13)	580(28)	0.4						

1.21 g cm^{-3} (12.5 mm) and 3.00 g cm^{-3} (18.0 mm), respectively.

In Table 2, it is possible to see that the internal validation for the four samples was very good, since the ^{226}Ra, ^{228}Ra and ^{228}Th activity concentrations calculated using the gamma emissions corresponding to their daughters (^{214}Pb and ^{214}Bi, ^{228}Ac and ^{212}Pb and ^{208}Tl, respectively) were very similar to each other for each one of those three radionuclides. Furthermore, note that for the Scale-1, Scale-2 and Tionite samples, there was clearly no secular equilibrium between ^{226}Ra and ^{238}U, given that the calculations at 186 keV were much better in the case of non-secular equilibrium. Regarding the Ilmenite sample, the opposite occurs than for the three previous samples, that is, at 186 keV the obtained calculations considering secular equilibrium were much better than the ones resulted from not considering it. This is very consistent since Ilmenite is a mineral and, consequently, secular equilibrium must be reached. For further information about chemical compositions of all the samples analyzed in this work, see Table A.9 (in Supplementary Information).

3.5. Analysis of ^{222}Rn losses in phosphogypsum and aqueous samples

Depending on the origin of the NORM sample (mineral, scale, waste obtained by precipitation, etc.), ^{226}Ra can be either distributed uniformly along the grains of the material or adsorbed onto the grains surface. For the phosphogypsum case, large ^{222}Rn losses have been observed and, consequently, significant disequilibria between ^{226}Ra and ^{222}Rn can be obtained (for further information about studies related to ^{222}Rn losses, see [54–59]. For this, the phosphogypsum samples previously studied (IAEA-434 and CSN-PG) have been selected. In order to study this issue, two ^{226}Ra measurements were made: one just after preparing them, and a second after waiting a month to assure ^{222}Rn and ^{226}Ra are in secular equilibrium (see Table 3).

Two thicknesses were chosen to analyze the ^{222}Rn losses in the IAEA-434 sample (where the volume of the cylindrical container is constant, the total interior height (H) is 60.5 ± 0.2 mm and the inner diameter ($\varnothing$) is 34.6 ± 0.2 mm). The obtained losses were 13 ± 4 % and 18 ± 3 % for h = 7.6 mm and 18.1 mm, respectively (average loss = 16 ± 3 %).

The CSN-PG sample was measured with a thickness of 15.4 mm, obtaining ^{222}Rn losses of 6 ± 3 % which are lower than the ones calculated in the case of the IAEA-434 sample. This fact could be related to the manufacturing procedure of the phosphogypsum samples. Probably, for the IAEA-434 sample, ^{226}Ra was more deposited onto the surface of the PG grains favoring the ^{222}Rn exhalation than in the CSN-PG, where the ^{226}Ra is more uniformly distributed inside the grains. Consequently, this fact allows us to recommend determining the ^{226}Ra activity concentration by using the 186 keV energy for samples whose ^{222}Rn exaltation rates from the grains are high (see Table 3).

Table 3 also shows the calculations of ^{226}Ra activity concentrations obtained using the 186 keV gamma emission for phosphogypsum materials. As it can be seen, these calculations are not only in very good agreement with respect to the reference values, but they are also better than the values calculated by the gamma emissions belonging to the ^{226}Ra daughters after waiting a month (see 2nd measure in Table 3).

To finish the study related to the determination of the radon losses from a sample, a liquid standard was prepared by dissolving a mass of RGU-1 containing 165.6 ± 5 Bq kg^{-1} of ^{238}U and h value being 30.3 mm (see Table 4). In this case, there was a very large ^{222}Rn loss due to its accumulation in the upper air chamber (where the thickness of the upper

Table 2
Internal validation for several NORM samples (Scale-1, Scale-2, Tionite and Ilmenite).

RN	E_γ(keV)	Scale-1	Scale-2	Tionite	Ilmenite
		a (Bq kg^{-1})	a (Bq kg^{-1})	a (Bq kg^{-1})	a (Bq kg^{-1})
^{234}Th	63.29	−49(54)	−55(26)	166(21)	135(17)
^{226}Ra	185.96 (Non-sec. eq.)	8658 (254)	2962(95)	562(26)	103(13)
	185.96 (Sec. eq.)	4906 (336)	1695 (118)	387(28)	115(9)
^{214}Pb	295.22	8744 (201)	2965(69)	537(13)	125(3)
	351.93	8607 (197)	2911(67)	538(13)	120(3)
^{214}Bi	609.31	8770 (203)	2911(68)	528(13)	120(3)
	1120.29	8825 (230)	3021(84)	550(18)	122(4)
^{228}Ac	338.42	3829 (651)	1997 (340)	2741 (466)	367(62)
	911.16	3884 (105)	2043(56)	2344(61)	485(13)
^{212}Pb	238.63	3082(69)	520(13)	364(8)	486(11)
^{208}Tl	583.19	3047(71)	513(15)	360(10)	472(10)

Table 3
Analysis of ^{222}Rn losses in phosphogypsum samples (IAEA-434 and CSN-PG). Determination of ^{226}Ra by 186 keV gamma emission in the IAEA-434 and CSN-PG samples in the case of secular non-equilibrium between ^{238}U and ^{226}Ra (Non-sec. eq.).

E_γ (KeV), RN	IAEA-434 (h = 7.6 mm)			z_{score}	
	a (Bq kg^{-1}) (1st measure)	a (Bq kg^{-1}) (2nd measure)	^{222}Rn losses (%)	(1st measure)	(2nd measure)
63 (^{234}Th)	156 ± 38				
186 (^{226}Ra, Non-sec. eq.)	766 ± 61			−0.2	
295 (^{214}Pb)	664 ± 24	692 ± 24	4 ± 5	−3.0	−2.3
352 (^{214}Pb)	648 ± 20	716 ± 21	10 ± 5	−3.6	−1.7
609 (^{214}Bi)	631 ± 21	732 ± 23	16 ± 5	−4.0	−1.3
1120 (^{214}Bi)	611 ± 46	751 ± 46	23 ± 12	−3.1	−0.5
		Average loss (%)	13 ± 4		
E_γ (KeV), RN	IAEA-434 (h = 18.1 mm)			z_{score}	
	a (Bq kg^{-1}) (1st measure)	a (Bq kg^{-1}) (2nd measure)	^{222}Rn losses (%)	(1st measure)	(2nd measure)
63 (^{234}Th)	−22 ± 24				
186 (^{226}Ra, Non-sec. eq.)	830 ± 77			0.6	
295 (^{214}Pb)	640 ± 22	732 ± 20	14 ± 5	−3.7	−1.3
352 (^{214}Pb)	641 ± 19	711 ± 18	11 ± 4	−3.8	−1.9
609 (^{214}Bi)	632 ± 20	724 ± 19	15 ± 5	−4.0	−1.5
1120 (^{214}Bi)	560 ± 37	734 ± 30	31 ± 10	−4.5	−1.1
		Average loss (%)	18 ± 3		
E_γ (KeV), RN	CSN-PG (h = 15.4 mm)			z_{score}	
	a (Bq kg^{-1}) (1st measure)	a (Bq kg^{-1}) (2nd measure)	^{222}Rn losses (%)	(1st measure)	(2nd measure)
63 (^{234}Th)	38 ± 14				
186 (^{226}Ra, Non-sec. eq.)	614 ± 35			−0.5	
295 (^{214}Pb)	536 ± 17	583 ± 17	9 ± 5	−2.1	0.1
352 (^{214}Pb)	555 ± 15	583 ± 15	5 ± 4	−1.3	0.1
609 (^{214}Bi)	535 ± 16	581 ± 16	9 ± 4	−2.2	0.1
1120 (^{214}Bi)	557 ± 29	571 ± 27	3 ± 7	−0.7	−0.3
		Average loss (%)	6 ± 3		

Table 4
Determination of ^{226}Ra by its daughters and 186 keV gamma emissions in dissolved RGU-1 standard in the case of secular non-equilibrium between ^{226}Ra and ^{222}Rn (h = 30.3 mm).

RN	E_γ(keV)	a (Bq kg^{-1})	Reference (Bq kg^{-1})	z_{score}
^{234}Th	63.29	183(15)	165.6(5)	1.1
^{226}Ra	185.96 (Secular equilibrium between ^{238}U and ^{226}Ra)	169(12)		0.3
^{214}Pb	295.22	53.5(1.7)		−62
	351.93	53.3(1.5)		−72
^{214}Bi	609.31	53.5(1.6)		−68
	1120.29	49(3)		−41

air chamber was 30.2 mm). For this sample, the average ^{222}Rn loss was 68 ± 5 % that was calculated comparing the ^{226}Ra activity concentrations, which were obtained using the gamma emissions of ^{214}Pb and ^{214}Bi, with the reference value. However, the ^{226}Ra activity concentration calculation using the 186 keV energy agreed very well with the reference value (see Table 4).

Furthermore, it is necessary to mention that the values of ^{222}Rn losses obtained in this Section are very consistent with the ones obtained in a previous study [30], where the percentages of the ^{222}Rn losses were 15(3) %, 11(2) % and 71(8) % for the IAEA-434, CSN-PG and dissolved RGU-1 samples, respectively.

4. Conclusions

In the present study, it has been developed a new method to calibrate in efficiency in order to determine natural γ- ray emitters in NORM samples using coaxial Ge detectors. For this, firstly the most intense gamma emissions (E_γ), which are characterized by not having interferences, of the radionuclides contained in the standards were chosen. Then, after compacting the standards until reaching the desired thickness values (h), the experimental values of the apparent full-energy peak efficiency (*FEPE*) were calculated for the different selected h and E_γ values. Finally, a function was chosen to fit the experimental *FEPEs* varying h (from 0.5 cm to 5 cm) and fixing E_γ, $\varepsilon_c(E_\gamma, h)$, which was an asymptotic exponential in this study, obtaining residues that were three times smaller than the ones obtained by other functions used in previous works. Regarding the comparison made between the experimental values calculated for *FEPE* and the ones provided by Genie 2000, very low average z_{score} values (less than 0.5) were obtained at all the selected energies, verifying both the good calculations carried out for experimental *FEPE* and the great reliability of the Genie 2000 software.

Then, it has been proved that the calibration in efficiency varying E_γ is less accurate than the one obtained varying h, since in the first case, the true coincidence summing effects are more relevant as well as the uncertainties of the experimental *FEPEs* increase due to the contribution of the gamma emission probability uncertainties. Besides, the residues resulted from the fittings done to calibrate varying E_γ were double than the ones obtained calibrating varying h. All this implies that the determination of artificial radionuclides would be more advisable to be carried out calibrating in efficiency by varying h and using standards which contain those artificial radionuclides instead of calibrating varying E_γ, that is, using the relative measurement of the activity.

On the other hand, it has been checked that the minimum detectable activity concentration (*mda*) decreases as the sample thickness (mass) increases as well as the *mda* depends on the characteristics (density and activity concentrations of ^{226}Ra and ^{228}Th) of each sample analyzed. In addition, at 186 keV *mda* values were higher when the secular equilibrium between ^{238}U and ^{226}Ra was not considered in comparison with the ones corresponding to the opposite case.

The methodology followed in this work has been validated employing several certified and non-certified NORM samples. Thus, in the internal validation, very similar activity concentration values were obtained for a specific radionuclide regardless of the E_γ selected to accomplish its determination, proving the good consistency of the proposed methodology. Besides, an external validation was carried out for certified samples, where the $|z_{score}|$ values resulted from this validation were less than 2, getting to fully check the very good validity of the methodology.

Finally, it has been demonstrated that the ^{226}Ra determination is much more recommendable to be carried out using its gamma emission (186 keV) than the ones corresponding to its daughters. This is especially true in samples characterized by having high ^{222}Rn losses such as phosphogypsum and aqueous samples, obtaining ^{222}Rn losses of 16 ± 3 %, 6 ± 3 % and 68 ± 5 % in the case of the IAEA-434, CSN-PG and dissolved RGU-1 samples, respectively, being these ^{222}Rn losses very consistent with the ones obtained in a previous work, where the same samples were analyzed.

CRediT authorship contribution statement

A. Barba-Lobo: Conceptualization, Data curation, Formal analysis, Investigation, Methodology, Validation, Writing – original draft, Writing – review & editing. **F. Mosqueda:** Conceptualization, Data curation, Formal analysis, Investigation, Methodology, Validation. **J.P. Bolívar:** Conceptualization, Data curation, Formal analysis, Investigation, Methodology, Supervision, Validation, Writing – original draft, Writing – review & editing.

Declaration of Competing Interest

The authors declare that they have no known competing financial interests or personal relationships that could have appeared to influence the work reported in this paper.

Acknowledgments

This research was partially funded by a project of the Regional Government of Andalusia “Basic processes regulating the fractionations and enrichments of natural radionuclides under acid mine drainage conditions” (Ref.: UHU-1255876), and a project of the Projects for Novel Principal Investigators “Quantitative study of the variables involved in the radon exhalation rate for granular solids; application to rafts of granular solid phosphogypsum” (Ref.: UHUPJ-00005-632). A.B.L. acknowledges support from funds provided by the Spanish Ministry of Science, Innovation and Universities’ Research Agency and co-financing provided by the European Social Fund (ESF) and the Spanish National Youth Guarantee Implementation Plan under Contract No. PEJ2018-002676-A. The authors acknowledge the funding for open access charge provided by Universidad de Huelva / CBUA.

Appendix A. Supplementary data

Supplementary data to this article can be found online at https://doi.org/10.1016/j.measurement.2021.110153.

References

[1] L. Barbero, M.J. Gázquez, J.P. Bolívar, M. Casas-Ruíz, A. Hierro, M. Baskaran, M. E. Ketterer, Mobility of Po and U-isotopes under acid mine drainage conditions: an experimental approach with samples from Río Tinto area (SW Spain), J. Environ. Radioact. 138 (2014) 384–389, https://doi.org/10.1016/j.jenvrad.2013.11.004.

[2] M.J. Gázquez, J. Mantero, F. Mosqueda, J.P. Bolívar, R. García-Tenorio, Radioactive characterization of leachates and efflorescences in the neighbouring areas of a phosphogypsum disposal site as a preliminary step before its restoration, J. Environ. Radioact. 137 (2014) 79–87, https://doi.org/10.1016/j.jenvrad.2014.06.025.

[3] V. Spasic Jokic, L. Zupunski, I. Zupunski, Measurement uncertainty estimation of health risk from exposure to natural radionuclides in soil, Measurement 46 (8) (2013) 2376–2383, https://doi.org/10.1016/j.measurement.2013.04.019.

[4] B. Michalik, G. de With, W. Schroeyers, Measurement of radioactivity in building materials – Problems encountered caused by possible disequilibrium in natural decay series, Constr. Build. Mater. 168 (2018) 995–1002, https://doi.org/10.1016/j.conbuildmat.2018.02.044.

[5] S. Abdualhadi, Quantifying Disequilibrium in U-Series Decay using High-Purity Germanium Spectrometry, Ph.D. Thesis (2016), University of Liverpool, https://core.ac.uk/download/pdf/80779313.pdf.

[6] B.A. Almayahi, A.A. Tajuddin, M.S. Jaafar, Effect of the natural radioactivity concentrations and $^{226}Ra/^{238}U$ disequilibrium on cancer diseases in Penang, Malaysia, Radiat. Phys. Chem. 81 (2012) 1547–1558, https://doi.org/10.1016/j.radphyschem.2012.03.018.

[7] M. Contreras, M.I. Martín, M.J. Gázquez, M. Romero, J.P. Bolívar, Valorisation of ilmenite mud waste in the manufacture of commercial ceramic, Constr. Build. Mater. 72 (2014) 31–40, https://doi.org/10.1016/j.conbuildmat.2014.08.091.

[8] J. Mantero, M.J. Gázquez, S. Hurtado, J.P. Bolívar, R. García-Tenorio, Application of gamma-ray spectrometry in a NORM industry for its radiometrical characterization, Radiat. Phys. Chem. 116 (2015) 78–81, https://doi.org/10.1016/j.radphyschem.2015.02.018.

[9] European Commission, Council Directive 2013/59/Euratom of 5 December 2013. Laying down basic safety standards for protection against the dangers arising from exposure to ionising radiation (1983), https://ec.europa.eu/energy/sites/ener/files/rp_188.pdf.

[10] R. Ravisankar, K. Vanasundari, A. Chandrasekaran, A. Rajalakshmi, M. Suganya, P. Vijayagopal, V. Meenakshisundaram, Measurement of natural radioactivity in building materials of Namakkal, Tamil Nadu, India using gamma-ray spectrometry, Appl. Radiat. Isot. 70 (4) (2012) 699–704, https://doi.org/10.1016/j.apradiso.2011.12.001.

[11] Z.s. Szabó, P. Völgyesi, H.É. Nagy, C.s. Szabó, Z. Kis, O. Csorba, Radioactivity of natural and artificial building materials – a comparative study, J. Environ. Radioact. 118 (2013) 64–74, https://doi.org/10.1016/j.jenvrad.2012.11.008.

[12] K. Krieger, NORM contamination - Now you see it, now you don't, Health Phys. 89 (2005) S20–S21. http://radonattahoe.com/TENORM.pdf.

[13] C. Tsabaris, E.G. Androulakaki, A. Prospathopoulos, S. Alexakis, G. Eleftheriou, D. L. Patiris, F.K. Pappa, K. Sarantakos, M. Kokkoris, R. Vlastou, Development and optimization of an underwater in-situ cerium bromide spectrometer for radioactivity measurements in the aquatic environment, J. Environ. Radioact. 204 (2019) 12–20, https://doi.org/10.1016/j.jenvrad.2019.03.021.

[14] Y.-Y. Ji, T. Lim, W. Lee, In Situ Gamma-ray Spectrometry Using an LaBr 3 (Ce) Scintillation Detector, J. Radiat. Prot. Res. 43 (2018) 85–96, https://doi.org/10.14407/jrpr.2018.43.3.85.

[15] E.G. Androulakaki, C. Tsabaris, F. Maragkos, D.L. Patiris, F.K. Pappa, G. Eleftheriou, S. Alexakis, M. Kokkoris, R. Vlastou, Calibration of a CeBr 3 based γ-spectrometer for onsite and laboratory radioactivity measurements in sediment samples, Appl. Radiat. Isot. 160 (2020) 109124, https://doi.org/10.1016/j.apradiso.2020.109124.

[16] V. Peyres, T. Crespo, M. Mejuto, E. García-Toraño, Measurement of NORM samples with CeBr 3 detectors, Appl. Radiat. Isot. 126 (2017) 307–310, https://doi.org/10.1016/j.apradiso.2017.02.012.

[17] C. Agarwal, S. Chaudhury, A. Goswami, M. Gathibandhe, Full energy peak efficiency calibration of HPGe detector for point and extended sources using Monte Carlo code, J. Radioanal. Nucl. Chem. 287 (2011) 701–708. https://link.springer.com/article/10.1007/s10967-010-0820-1.

[18] Z. Ahmed, In-Situ object calibration software (ISOCS) technique for ^{235}U mass verification, Measurement 145 (2019) 648–650, https://doi.org/10.1016/j.measurement.2019.05.058.

[19] G. Eleftheriou, C. Tsabaris, E.G. Androulakaki, D.L. Patiris, M. Kokkoris, C. A. Kalfas, R. Vlastou, Radioactivity measurements in the aquatic environment using in-situ and laboratory gamma-ray spectrometry, Appl. Radiat. Isot. 82 (2013) 268–278, https://doi.org/10.1016/j.apradiso.2013.08.007.

[20] N.L. Maidana, V.R. Vanin, J.A. García-Álvarez, M. Hermida-López, L. Brualla, Experimental HPGe coaxial detector response and efficiency compared to Monte Carlo simulations, Appl. Radiat. Isot. 108 (2016) 64–74, https://doi.org/10.1016/j.apradiso.2015.12.001.

[21] B. Quintana, M.C. Pedrosa, L. Vázquez-Canelas, R. Santamaría, M.A. Sanjuán, F. Puertas, A method for the complete analysis of NORM building materials by γ-ray spectrometry using HPGe detectors, Appl. Radiat. Isot. 134 (2018) 470–476, https://doi.org/10.1016/j.apradiso.2017.07.045.

[22] H. Zhu, R. Venkataraman, W. Mueller, J. Lamontagne, F. Bronson, K. Morris, A. Berlizov, X-ray true coincidence summing correction in Genie, Appl. Radiat. Isot. 67 (2009) (2000) 696–700, https://doi.org/10.1016/j.apradiso.2009.01.013.

[23] J.A. Suárez-Navarro, C. Gascó, M.M. Alonso, M.T. Blanco-Varela, M. Lanzon, F. Puertas, Use of Genie 2000 and Excel VBA to correct for γ-ray interference in the determination of NORM building material activity concentrations, Appl. Radiat. Isot. 142 (2018) 1–7, https://doi.org/10.1016/j.apradiso.2018.09.019.

[24] Canberra Industries, Genie 2000 Spectroscopy software: Customization tools, Printed in the United States of America (2004), http://depni.sinp.msu.ru/~hatta/canberra/Genie%202000%20Customization%20Tools%20Manual.pdf.

[25] IAEA, Reference products for environment and trade: Natural radionuclide activity concentrations, RGU-1 (1987), https://www.google.com/url?sa=t&rct=j&q=&esrc=s&source=web&cd=&cad=rja&uact=8&ved=2ahUKEwjxqaS6rfnpAhUL8BQKHU2cBMEQFjAAegQIBBAB&url=http%3A%2F%2Fisostandards-crm.com%2Fdocumentos%2Fproductos%2Fcoa%2FIAEA-RGU-1.pdf&usg=AOvVaw2ukbHpx9MsYFGxoirUTIhf.

[26] IAEA, Preparation of gamma-ray spectrometry reference materials RGU-1, RGTh-1 and RGK-1. Report-IAEA/RL/148, Vienna (1987), https://nucleus.iaea.org/sites/ReferenceMaterials/Shared%20Documents/ReferenceMaterials/Radionuclides/IAEA-RGTh-1/rl_148.pdf.

[27] H. Wiedner, J. Riedl, F.J. Maringer, A. Baumgartner, M. Stietka, F. Kabrt, Production and characterization of a traceable NORM material and its use in proficiency testing of gamma-ray spectrometry laboratories, Appl. Radiat. Isot. 134 (2018) 45–50, https://doi.org/10.1016/j.apradiso.2017.09.025.

[28] The Decay Data Evaluation Project, http://www.nucleide.org/DDEP_WG/DDEPdata.htm.

[29] G. Gilmore, J. Hemingway, Practical gamma-ray spectrometry, John Wiley & Sons, Chichester (1995), https://doi.org/10.1002/rcm.1290091227.

[30] A. Barba-Lobo, E.G. San Miguel, R.L. Lozano, J.P. Bolívar, A general methodology to determine natural radionuclides by well-type HPGe detectors, Measurement 181 (2021) 109561, https://doi.org/10.1016/j.measurement.2021.109561.

[31] Y. Venegas-Argumedo, M.E. Montero-Cabrera, True coincidence summing corrections for an extended energy range HPGe detector, AIP Conf. Proc. 1671 (2015), 030004, https://doi.org/10.1063/1.4927193.

[32] K. Debertin, R.G. Helmer, Gamma- and X-ray spectrometry with semiconductor detectors, Elsevier, Amsterdam, 1988 https://inis.iaea.org/search/search.aspx?orig_q=RN:20046286.

[33] MATLAB: Algorithms employed for the fittings (2021), https://es.mathworks.com/help/optim/ug/equation-solving-algorithms.html?lang=en.

[34] P.R. Bevington, D. Keith, Data reduction and error analysis for the physical sciences, McGraw-Hill, New York, 1969 https://www.scirp.org/(S(i43dyn45teexjx455qlt3d2q))/reference/ReferencesPapers.aspx?ReferenceID=1813409.

[35] P. Jodłowski, Self-absorption correction in gamma-ray spectrometry of environmental samples – an overview of methods and correction values obtained for the selected geometries, Nukleonika 51 (2006) 21–25. https://www.nukleonika.pl/www/back/full/vol51_2006/v51s2p21f.pdf.

[36] M.L. Montes, M.G. Rizzoto, J. Juri Ayub, R. Torres Astorga, M.A. Taylor, An alternative methodology to determine 210Pb activity soil profiles, J. Environ. Radioact. 208-209 (2019) 105998, https://doi.org/10.1016/j.jenvrad.2019.105998.

[37] J.P. Pérez-Moreno, E.G. San Miguel, J.P. Bolívar, J.L. Aguado, A comprehensive calibration method of Ge detectors for low-level gamma-spectrometry measurements, Nucl. Instrum. Methods Phys. Res. A 491 491 (1-2) (2002) 152–162, https://doi.org/10.1016/S0168-9002(02)01165-8.

[38] J.A. Suárez-Navarro, A.M. Moreno-Reyes, C. Gascó, M.M. Alonso, F. Puertas, Gamma spectrometry and LabSOCS-calculated efficiency in the radiological characterisation of quadrangular and cubic specimens of hardened portland cement paste, Radiat. Phys. Chem. 171 (2020) 108709, https://doi.org/10.1016/j.radphyschem.2020.108709.

[39] J.P. Bolivar, R. García-Tenorio, M. García-León, Radioactive Impact of some Phosphogypsum Piles in Soils and Salt Marshes Evaluated by γ-Ray Spectrometry, Appl. Radiat. Isot. 47 (9-10) (1996) 1069–1075, https://doi.org/10.1016/S0969-8043(96)00108-X.

[40] F. El-Daoushy, R. Garcia-Tenorio, Well Ge and semi-planar Ge (HP) detectors for low-level gamma-spectrometry, Nucl. Instrum. Methods Phys. Res. A 356 (2-3) (1995) 376–384, https://doi.org/10.1016/0168-9002(94)01351-9.

[41] F. Martínez-Ruiz, E. Borrego, E.G. San Miguel, J.P. Bolívar, An efficiency calibration for ^{210}Pb and ^{7}Be measurements by gamma-ray spectrometry in atmospheric filters, Nucl. Instrum. Methods Phys. Res. A 580 (2007) 663–666, https://doi.org/10.1016/j.nima.2007.05.117.

[42] M.R. Zare, M. Kamali, Z. Omidi, M. Fallahi-Kapourchali, Designing and producing large-volume liquid gamma-ray standard sources for low radioactive pollution measurements of seawater samples by comparison between experimental and simulation results, Measurement 90 (2016) 412–417, https://doi.org/10.1016/j.measurement.2016.04.065.

[43] A. Barba-Lobo, F. Mosqueda, J.P. Bolívar, A general function for determining mass attenuation coefficients to correct self-absorption effects in samples measured by gamma spectrometry, Radiat. Phys. Chem. 179 (2021) 109247, https://doi.org/10.1016/j.radphyschem.2020.109247.

[44] M. Bonczyk, Determination of ^{210}Pb concentration in NORM waste – An application of the transmission method for self-attenuation corrections for gamma-ray spectrometry, Radiat. Phys. Chem. 148 (2018) 1–4, https://doi.org/10.1016/j.radphyschem.2018.02.011.

[45] J.G. Guerra, Caracterización computacional de detectores de Germanio Hiperpuro (HPGe) empleando simulación Montecarlo y optimización mediante algoritmos evolutivos, Ph.D. Thesis (2018), University of Las Palmas de Gran Canaria, https://hdl.handle.net/10553/55862.

[46] E.G. San Miguel, J.P. Pérez-Moreno, J.P. Bolívar, R. García-Tenorio, J.E. Martin, ^{210}Pb determination by gamma spectrometry in voluminal samples (cylindrical

geometry), Nucl. Instrum. Methods Phys. Res. A 493 493 (1-2) (2002) 111–120, https://doi.org/10.1016/S0168-9002(02)01415-8.
[47] M. Xhixha-Kaçeli, New gamma-ray spectrometry methods for estimating K, U, Th concentrations in rocks of the Sardinia Batholith, Ph.D. Thesis (2013), University of Sassari, https://core.ac.uk/reader/19979790.
[48] Norman H. Cutshall, Ingvar L. Larsen, Curtis R. Olsen, Direct analysis of ^{210}Pb in sediment samples: Self-absorption corrections, Nucl. Instrum. Methods Phys. Res. A 206 (1-2) (1983) 309–312, https://doi.org/10.1016/0167-5087(83)91273-5.
[49] NIST Standard Reference Database 126 (2004), https://physics.nist.gov/PhysRefData/XrayMassCoef/tab3.html.
[50] XCOM, National Institute of Standards and Technology (NIST), https://physics.nist.gov/PhysRefData/Xcom/html/xcom1.html.
[51] J.P. Bolívar, Aplicaciones de la espectrometría gamma y alfa al estudio del impacto radiactivo producido por industrias no nucleares, Ph.D. Thesis (1995), University of Seville, https://idus.us.es/handle/11441/15757;jsessionid=42BB498B6CEA3B51479807DD80A23830?.
[52] Ll.A. Currie, Limits for qualitative detection and quantitative determination. Application to radiochemistry, Anal. Chem. 40 (1968) 586–593, https://doi.org/10.1021/ac60259a007.
[53] A.R. Agha, S.A. El-Mongy, A.E. Kandel, Assay of uranium isotopic ratios 234U/238U, 235U/238U in bottom sediment samples using destructive and non destructive techniques (Nasser Lake), Proceedings of the eighth Nuclear and Particle Physics Conference (NUPPAC-2011) 43 (2011) 221-229, https://inis.iaea.org/search/search.aspx?orig_q=RN:43099476.
[54] R.R. Benke, K.J. Kearfott, Accounting for ^{222}Rn loss during oven drying for the immediate laboratory gamma-ray spectroscopy of collected soil samples, Appl. Radiat. Isot. 52 (2000) 271–287, https://doi.org/10.1016/S0969-8043(99)00144-X.
[55] J.H. Hightower, J.E. Watson, 222Rn in water: a study of two sample collection methods, effects of mailing samples, and temporal variation of concentrations in North Carolina groundwater, Health Phys. 69 (2) (1995) 219–226, https://doi.org/10.1097/00004032-199508000-00006.
[56] Predrag Kuzmanović, Nataša Todorović, Sofija Forkapić, Leposava Filipović Petrović, Jovana Knežević, Jovana Nikolov, Bojan Miljević, Radiological characterization of phosphogypsum produced in Serbia, Radiat. Phys. Chem. 166 (2020) 108463, https://doi.org/10.1016/j.radphyschem.2019.108463.
[57] F. Lamonaca, V. Nastro, A. Nastro, D. Grimaldi, Monitoring of indoor radon pollution, Measurement 47 (2014) 228–233, https://doi.org/10.1016/j.measurement.2013.08.058.
[58] J.C. Scholten, I. Osvath, M. Khanh-Pham, ^{226}Ra measurements through gamma spectrometric counting of radon progenies: How significant is the loss of radon? Mar. Chem. 156 (2013) 146–152, https://doi.org/10.1016/j.marchem.2013.03.001.
[59] K. Tudyka, F. Pawelczyk, A. Michczyński, Bias arising from ^{222}Rn contamination in standardized methods for biobased content determination and a simple removal method, Measurement 167 (2021), 108263, https://doi.org/10.1016/j.measurement.2020.108263.